# Dissolving microneedle patch loaded with adipokines-enriched adipose extract relieves atopic dermatitis in mouse via modulating immune disorders, microbiota imbalance, and skin barrier defects

Jingyan Guan*[iD], Kaiqi Chen*, Feng Lu and Yunfan He[iD]

## Abstract

Atopic dermatitis (AD) is a chronic relapsing dermatosis that demands new therapies. This research group previously developed a physically extracted adipose-derived extracellular matrix named adipose collagen fragments (ACF), which was determined containing massive adipose matrix-bound adipokines and medicable on AD through intradermal injection. However, problems concerning the control of drug release and inevitable pain caused by injection hinder the application of ACF in clinics. Microneedle (MN) is a rapid developing technique for precise and painless transdermal drug delivery. Therefore, a dissolving methacrylated gelatin/hyaluronic acid MN patch loaded with ACF was developed in this study. The morphological characteristics, mechanical properties, penetration ability, as well as biocompatibility and degradation efficiency of ACF-MN were evaluated, and its efficacy on ovalbumin-induced AD mice was also investigated. ACF-MN exhibited excellent penetration ability, biocompatibility, degradation efficiency, and satisfying efficacy on murine AD similar with fresh-made ACF. Furthermore, RNA-Seq combining bioinformatics were performed for mechanism exploration. ACF treatment showed a comprehensive efficacy on AD via restoring inflammatory dysregulation, microbiota imbalance, and skin barrier defects. This study offered a novel MN-based ACF-bound adipokines transdermal delivery system that may serve as a promising strategy for relieving AD.

Department of Plastic and Cosmetic Surgery, Nanfang Hospital, Southern Medical University, Guangzhou, Guangdong, P.R. China

*These authors contributed equally to this work.

**Corresponding authors:**

Feng Lu, Department of Plastic and Cosmetic Surgery, Nanfang Hospital, Southern Medical University, 1838 Guangzhou North Road, Guangzhou, Guangdong 510515, P.R. China.
Email: doctorlufeng@hotmail.com

Yunfan He, Department of Plastic and Cosmetic Surgery, Nanfang Hospital, Southern Medical University, 1838 Guangzhou North Road, Guangzhou, Guangdong 510515, P.R. China.
Email: doctorheyunfan@hotmail.com

**Graphical abstract**
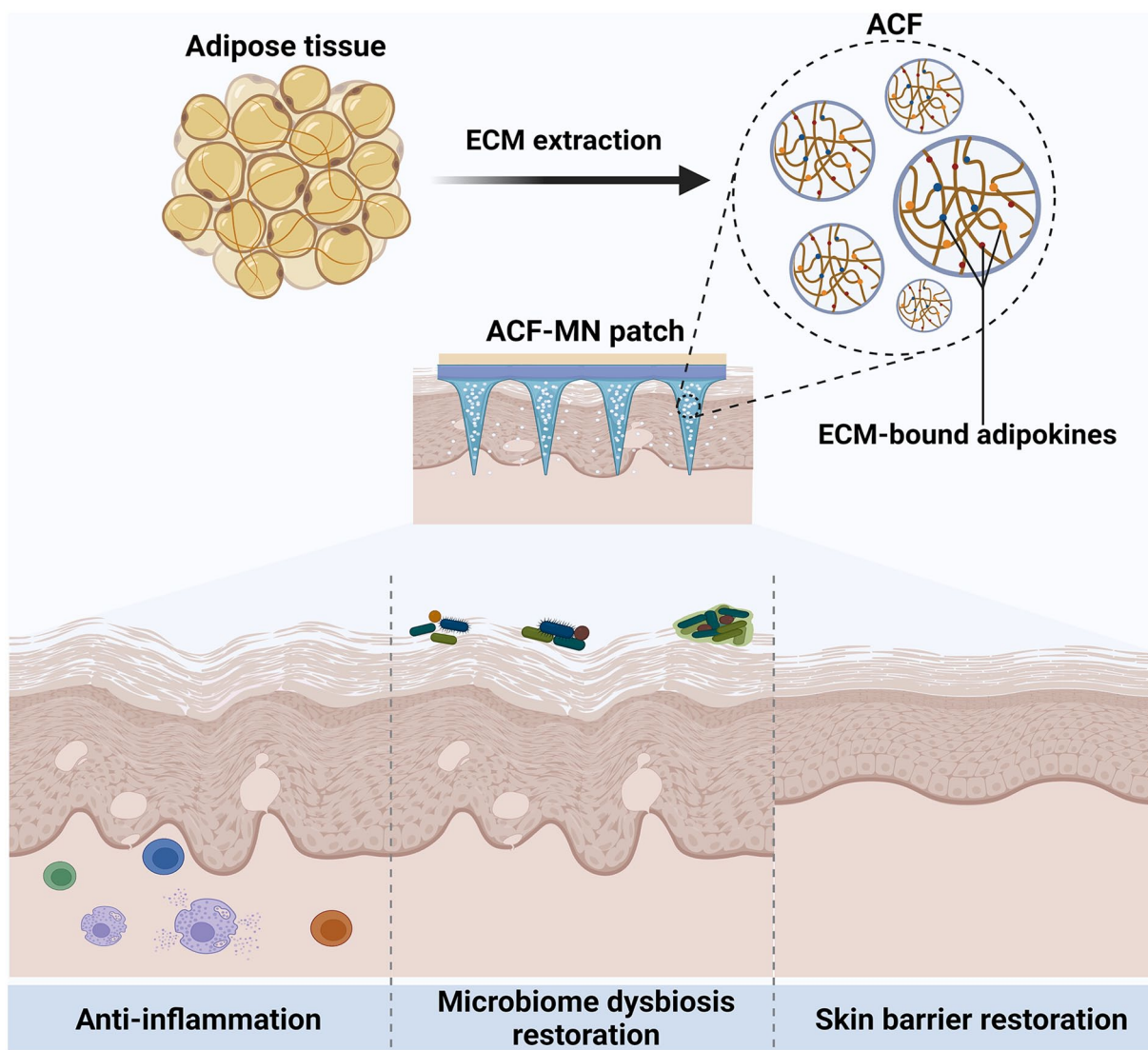


## Introduction

As a global common chronic inflammatory dermatosis which affects 1%–20% of individuals worldwide,[1] atopic dermatitis (AD) is characterized by insufferable pruritus and recurrent eczematous lesions. Pathogenesis of AD involves complex interactions among immune disorders, skin barrier dysfunction, and skin microbiome dysbiosis.[2] It has been demonstrated that the cross talk among these pathogenic factors would form a vicious feedback loop that aggravate AD symptoms.[3] Nowadays, although glucocorticoids and immunosuppressive agents remain the first-line strategies for AD treatment. These medications have been studied to reduce the inflammatory response by suppressing multiple inflammatory genes immune pathways.[4–6] However, Most patients often respond poorly to glucocorticoid therapy, especially in long-term use.[7–9] For

many patients, systemic treatment with immunosuppressants may not be successful, and the associated side effects limit their wide usage.[10] Thus, development of safer and more effective therapeutic options for AD are needed to address these limitations.

Skin is the largest and outmost organ in the body with multiple anatomical layers includes epidermis, dermis, and adipose tissue, which have been illustrated involving in skin defense via various specific mechanisms. Particularly, the skin adipose tissue, which did not used to be considered as an important player of skin defense, has attracted increasing attention in maintaining skin homeostasis by secreting various biological signaling factors termed "Adipokines." Therefore, the recognition of adipose tissue as an endocrine organ capable of storing adipokines has led to a series of studies on adipose tissue-based therapy in the past decade.[11,12] Importantly, it has been shown that

subcutaneous adipose tissue continually benefits the skin micro-environment via the secretion of adipokines.[13,14] Thus, adipose tissue-derived adipokines appear to be promising therapeutic agents for the alleviation of AD.

Our research group previously developed a physically extracted adipose-derived extracellular matrix (ECM) named adipose collagen fragments (ACF).[15] And our previous study illustrated that ACF contains abundant adipose ECM-bound adipokines with multiple biological function through proteomic analysis,[16] and its curative effect on AD was also demonstrated through in vivo animal experiments.[17] Using an ovalbumin (OVA)-induced AD mouse model, intradermally injection of ACF was found to ameliorated AD skin lesions by improving skin barrier function and inflammatory dysregulation.[17] Therefore, ACF may serve as a promising option for the treatment of AD. However, as a recurrent inflammatory disease, the skin lesions of patients with AD are prone to thickening at the chronic stage, which significantly decreases the topical permeability of the delivered drugs.[18] Although topical injection of drugs is generally used to relieve pruritus and pain in AD patients, it inevitably provokes significant pain, and the control of injection depth, drug release, and administered dose is challenging in clinics. Thus, a more precise transdermal delivery strategy of ACF with less invasive manner is required

The development of the microneedle (MN) technique has recently attracted increasing interest in the field of dermatoses.[19–24] The MN patch is considered an emerging transdermal drug delivery system that provides invasive, painless, and controlled transdermal drug delivery.[25–28] Traditional solid MN has limited delivery efficacy due to passive diffusion of the drug through the microchannel.[29] Dissolving MN encapsulates drugs in biodegradable matrix and delivers drugs beneath the skin after penetration, eliminating the creation of biohazardous waste. Therefore, in the present study, a dissolving MN patch loaded with ACF-derived adipokines (ACF-MN patch) was proposed. Methacrylated gelatin (Gel-MA) is originated from natural hydrogel gelatin and has advantages in lower fabrication cost and higher production yield, making it an ideal candidate for translational studies in skin care comparing to other nature-derived material.[30] Due to its excellent biocompatibility, biodegradability, mechanical property, non-immunogenicity, and water-solubility, hyaluronic acid (HA) was also chosen as the matrix to prepare dissolvable MN patch.[31] In this study, the ACF-MN patches were developed by incorporating ACF in Gel-MA/HA, and the morphological characteristics, mechanical properties, penetration, and insertion ability of the ACF-MN patches were studied. Furthermore, using OVA-induced AD mouse model, the therapeutic efficacy of ACF-MN patches was evaluated, and sequencing techniques combining bioinformatic analysis were performed to investigate the underlying mechanism.

## Materials and methods

### Animals and ACF preparation procedure

The preparation of ACF was conducted using adipose tissue from 6-week-old female BALB/c mice which were purchased from the Nanfang Hospital Animal Center (Guangzhou, China). The Nanfang Hospital Animal Ethic Committee approved all animal procedures. Following the guidelines of the National Health and Medical Research Council (People's Republic of China), all animal operations were conducted under aseptic conditions. BALB/c mice were euthanized and shaved for adipose tissue harvesting. About 1.5 g of inguinal fat was isolated from each mouse. To remove red blood cells, the isolated fat was washed twice with phosphate buffer solution (PBS, pH 7.4). The fat was then cut into small pieces using sterile scissors and centrifuged (200$g$, 5 min), and the liquid portion was discarded. Using a high-speed homogenizer (FSH-2A; Chongqing Kanghui Instruments Co., Ltd., Chongqing, China), the adipose tissue was homogenized for 1 min at 10,000 rpm/min, followed by filtered through 0.25 and 0.15 mm stainless steel meshes consecutively to remove large fibrous segments. After being centrifuged for 3 min at 3000$g$, collagen precipitate, which was defined as ACF, was isolated from the adipose tissue suspension (Figure 1(a)). Then the ACF was collected for the following experiments.

### Fabrication of ACF-MN patch

Polydimethylsiloxane (PDMS) molds (Dow Corning, Midland, MI) with $12 \times 12$ MN arrays were used to fabricate ACF-MNs. The center-to-center spacing, base diameter, height, and tip diameter of each MN groove were 1000, 460, 1000, and 15 μm, respectively. Firstly, 1 g of Gel-MA (Sigma-Aldrich, St. Louis, MO, USA) and 0.1 g of HA (Sigma-Aldrich) were first mixed together and dissolved with 10 ml of 0.1% photo-initiator. Then ACF was added to the Gel-MA/HA solution at different mass ratios (1:1, 2:1, and 3:1) and dispersed using ultrasonic vibration, and then 200 μl of each casting solution was added to the top of the PDMS mold. Subsequently, the PDMS molds were placed in vacuum for 5 min, followed by ultraviolet irradiation for 2 min and desiccant drying at 4°C for 5 h. Subsequently, the PDMS molds were cleaned and cast with 200 μl of the second casting solution, which consisted of 10% polyvinyl alcohol (PVA, w/v, Lakeshore Biomaterials Inc., AL, USA) and 20% gelatin (w/v, Sigma-Aldrich). The molds were then vacuumed for 5 min, followed by 24 h of drying at 4°C using desiccant. Finally, adhesive papers were placed on the top surface of the PDMS molds, and the ACF-MNs were carefully demolded (Figure 1(b)). The ACF-MN patches were stored with desiccant in 4°C until being used.
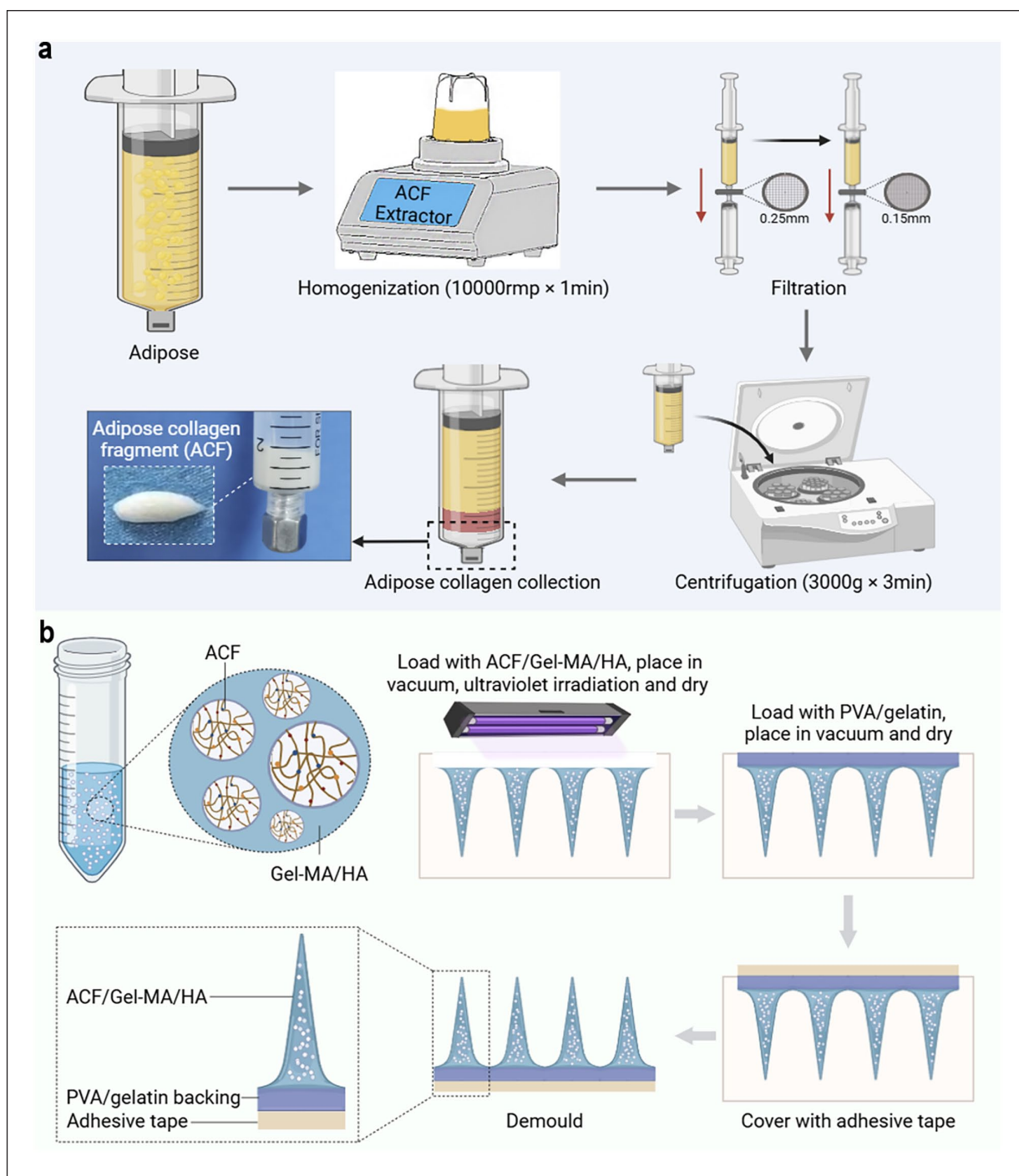
**Figure 1.** Preparation of ACF and fabrication of ACF-MN patches. (a) Schematic of the process of ACF preparation. (b) Schematic of the process of ACF-MN patches fabrication.

## Morphology characterization of ACF-MN patch, fracture force, in vitro release profile and skin insertion studies

The microscopic features of ACF-MNs were captured using an optical microscope (GP-304K, Gaopin, Dongguan, Guangdong, China) and scanning electron microscope (SEM, FEI, Quanta 200, Oregon, USA). The center-to-center spacing, height, base diameter, and tip diameter of the fabricated ACF-MNs ($n = 10$ each) were measured utilizing ImageJ software (NIH, Bethesda, MD, USA). The fracture force of ACF-MNs with different mass ratios of ACF to Gel-MA/HA solution was measured by conducting uniaxial compression tests utilizing a displacement force test station (Force Gauge, Mark-10, Copiague, NY, USA).

According to the fracture force determined above, ACF-MN patch with optimal ACF/Gel-MA/HA ratio was chosen to perform the ex vivo skin insertion test. Briefly, the ACF-MN patches were pressed vertically into the excised mouse skin and left for a series of predetermined time periods (5, 10, 30, and 60 min). After removal of the ACF-MN patches, the excised mouse skin was stained with 4% trypan blue solution for 10 min to confirm the formation of microchannels. The excised mouse skin was fixed with 10% formalin, embedded in paraffin, and cut into 4 μm thick sections for hematoxylin and eosin (H&E) staining. The remaining ACF-MN patches removed at predetermined times were observed under an optical microscope, and MNs with incomplete tips were considered to have been inserted into the skin. ACF-MN insertion efficiency was evaluated as insertion rate, measured using the following formula: Insertion rate =

$$\frac{\text{number of inserted MN}}{\text{total number of MN in a patch (144)}} \times 100\%$$

## Anti-inflammatory and immunomodulatory effects of ACF extraction in vitro

Mouse monocyte macrophage leukemia cells, RAW264.7 were prepared and incubated in culture dish at 37°C until cells were attached to the wall. Then serum-free medium was added to the culture dish and incubate for 4 h and a new medium was introduced to stimulate the production of inflammatory factors in RAW264.7 cells using Lipopolysaccharides (LPS). Simultaneously, different microneedle patches,with mass ratios of ACF to the Gel-MA/HA solution (1:1, 2:1, and 3:1), were added to incubate the RAW264.7 cells for 48 h. The cells were harvested and subjected to ultrasonic waves to release their internal contents. The supernatant was then collected by centrifugation and the inflammatory factors (TNF-α and IL-6) were tested using the ELISA kit (Jiangsu Meimian Industrial Co., Ltd).

## In vivo application of ACF-MN patches

To evaluate the biosafety of ACF-MNs, ACF-MN patches were first applied to healthy mice. Briefly, female BALB/c mice (six-week-old) were shaved, and the ACF-MN patches were applied to the dorsal surface and removed after 30 min. The cutaneous reaction caused by the ACF-MN patches was observed until 7 days after application. To evaluate the release rate of ACF from the MN patch in vivo, ACF-MN patches with fluorochromes were applied to healthy mice. Briefly, 5% Nile red dye (w/v) was added to a 2:1 ACF/Gel-MA/HA solution and mixed well using ultrasonic vibration. The solution labeled with Nile red dye was used to fabricate fluorescent ACF-MN patches following the same procedures as the regular ACF-MN patches. Fluorescent ACF-MN patches were then applied to the dorsal skin of shaved

female BALB/c mice (six-week-old) for 30 min. An in vivo imaging system (Spectral Lago X; Spectral Instruments Imaging, USA) was used to capture and measure the fluorescence area were meat the application site on days 0, 1, 3, 7, and 10.

## AD mouse model preparation and treatment

To assess the therapeutic effect of ACF-MN patch on AD, four groups (*n* = 6 per group) were set in the present study: (a) Balb/c mice without AD induction (normal control group), (b) AD-induced Balb/c mice treated with PBS (PBS group), (c) AD-induced Balb/c mice treated with freshly made ACF (ACF group), and (d) AD-induced Balb/c mice treated with ACF-MN patch (ACF-MN group). The AD-like skin lesion was induced by repeated epidermal challenges with OVA according to a standard protocol.[32] Briefly, 6-week-old female BALB/c mice were firstly anesthetized with isoflurane and shaved. Tegaderm 3M tape (Owens and Minor, Mechanicsville, VA, USA) was used to stripped the mice dorsal skin for six times, followed by skin sensitization using 1 cm × 1 cm sterile gauze soaked with 100 μg/100 μl OVA/saline solution. Each mouse was subjected to three rounds of OVA sensitization for 1 week with 2-week intervals.

On days 28 and 35 during the sensitization period, 0.1 ml of ACF or PBS was intradermally injected to the dorsal skin (sensitization sites) of mice in ACF group and PBS group, respectively. And ACF-MN patches were applied to the same area of mice in ACF-MN group for 30 min and then removed. On day 50, the transepidermal water loss (TEWL) level of the mouse dorsal skin was measured using a Vapo Scan AS-VT100RS machine (ASCH Japan Co., Ltd., Tokyo, Japan) at room temperature (25°C–30°C) and room humidity (50%–60%), and skin microbiome samples were collected using swabs. Thereafter, the mice of each group were euthanized, and dorsal skins were collected. For each mouse, half of the dorsal skin was stored at −80°C, and the other half was fixed in 10% formalin for further analyses.

## Assessment of AD symptom severity

The severity of AD was assessed by six symptoms as follow: erythema/hemorrhage, crust/excoriation, oozing/erosion, swelling/edema, dryness, and lichenification. Each symptom was rated from 0 (none) to 3 (severe). The assessment was performed by two independent investigators, and the severity of AD was measured as the average of sum scores.

## Histological examination

Paraffin was applied to embed the dorsal skin samples that were fixed in 10% formalin, before sectioning them to a thickness of 4 μm. The tissue sections were stained with

H&E and toluidine blue (TB), followed by observation under a microscope (20 ×, Olympus Corp., Tokyo, Japan). Using ImageJ software (NIH, Bethesda, MD, USA), epidermal thickness was measured from H&E-stained sections, and infiltrated mast cells were counted from TB-stained sections (10 sites/group).

### RNA-Seq analyses of skin samples

RNA-Seq analyses was applied in the NC group, PBS group, and ACF group ($n = 3$/group). Total RNA was first extracted with TRIzol Reagent® (Invitrogen, Carlsbad, CA, USA), then qualified by Agilent Bioanalyzer 2100 system (Agilent Technologies, Santa Clara, CA, USA). Poly-T oligo-attached magnetic beads were used for RNA Purification, and the purified RNA was reverse transcribed into cDNA. PCR was performed after the cDNA being ligated with adaptors, followed by library construction of each sample. Sequencing of the libraries was performed on Illumina Hiseq 3000 (Illumina, San Diego, CA, USA) platform with 150-bp paired-end reads. Using in-house Perl scripts, raw fastq reads were processed into clean reads. Alignment was performed with Mus musculus (mm10) as the reference genome sequence. Subsequently, read counts of each gene were computed utilizing FeatureCounts (v1.5.0-p3). Differential expression analysis and enrichment analysis was conducted using R software (v3.5.1). Using "EdgeR" R package (v1.20.0), with a threshold of adjusted $p$ value ($p$adj) $\leq 0.05$ and |log2 fold change (FC)| $\geq 1$, differentially expressed genes (DEGs) were identified. "ClusterProfiler" R package was used for Kyoto Encyclopedia of Gene and Genome (KEGG) enrichment analysis of DEGs, and pathway with $p$adj $< 0.05$ was considered significantly enriched. Gene Set Enrichment Analysis (GSEA) was performed on https://www.gsea-msigdb.org/gsea/index.jsp

### Quantitative real-time polymerase chain reaction (qPCR)

The RNA of skin samples was extracted using TRIzol reagent (Invitrogen, Carlsbad, CA, USA), followed by cDNA synthesizing using a reverse transcription kit (DBI Bioscience, Hennigsdorf, Germany). Then using a FastStart Universal SYBR Green Master Mix (Cat No. 04913850001; Roche, Basel, Switzerland), qPCR was performed. Using ΔΔCt method with β-actin (Forward: GAGGTATCCTGACCCTGAAGTA, Reverse: CACA CGCAGCTCATTGTAGA) acting as the endogenous reference gene, the relative gene expression levels of the following mentioned cytokines were measured: interferon-gamma (IFN-γ; Forward: ATCGGCTGACCTAGA GAAGA, Reverse: AGCCAAGATGCAGTGTGTAG), tumor necrosis factor-alpha (TNF-α; Forward: CTAC CTTGTTGCCTCCTCTTT, Reverse: GAGCAGAGGTTC

AGTGATGTAG), interleukin (IL)-4 (Forward: GACG GCACAGAGCTATTGAT, Reverse: GGATATGGCTCCT GGTACATTC), IL-13 (Forward: GCTGAGCAACATCAC ACAAG, Reverse: AATCCAGGGCTACACAGAAC), and IL-17 (Forward: CAAACATGAGTCCAGGGAGAG, Reverse: GCTGAGCTTTGAGGGATGAT).

### 16S-targeted amplicon sequencing

Microbial samples were first collected from mice dorsal skins by swabs ($n = 3$ per group), then following the manufacturer's instructions, a DNA isolation kit (GHFDE100, GUHE Laboratories, Hangzhou, China) was used to extract total bacterial genomic DNA. After quantification and qualification of the extracted DNAs, the bacterial 16S rRNA genes V4 region were amplified by PCR, with a forward primer 515F (5′-GTGCCAGCMGCCGCGGTAA-3′) and the reverse primer 806R (5′-GGACTACH VGGGTWTCTAAT-3′). PCR amplicons were then purified using Agencourt AMPure XP Beads (Beckman Coulter, Indianapolis, IN) and quantified with PicoGreen dsDNA Assay Kit (Invitrogen, Carlsbad, CA, USA). After being pooled in equal amounts, amplicons were conducted pair-end $2 \times 150$ bp sequencing using the Illumina NovaSeq6000 platform. Raw sequencing reads that matched to the barcodes were identified as valid sequences. Sequences with an average quality of $Q \leq 20$ per 4 bp or below 50 bp were filtered. Low-quality sequences with an average quality of $Q \leq 20$ per 4 bp or reads below 50 bp were filtered. Assembling of paired-end reads was performed using Vsearch v2.4.4, and operational taxonomic units (OTUs) was picked using Vsearch v2.15.0. Process of OTUs and data sequencing were conducted using QIIME2 pipeline (v2020.6). SILVA138 database was employed to classify OTU taxonomy. Sequence data analyses were performed on Microbiomeanalyst (https://www.microbiomeanalyst.ca/). Microbial richness was determined as OTU-level alpha diversity (Chao1 richness estimator), which was calculated in QIIME2. Taxa abundances at genus level among groups were compared by one-way ANOVA, with $p \leq 0.05$ was considered statistically significant. And LEfSe was used to calculate the differentially abundant taxa among groups.

### Liquid chromatography-mass spectrometry (LC-MS) analyses

The lipid of skin sample was extracted for analysis. The skin sample was incubated overnight in 2.5 mg/ml DISPASE® (Sigma-Aldrich) at 4°C, followed by separating the epidermis from the whole layer skin enzymatically. Then the lipid was extracted from the epidermis following a procedure as previously described.[33] Using ultraperformance liquid chromatography on an ACQUITY UPLC® BEH C18 column (1.7 μm, 2.1 mm × 100 mm) coupled to

a Waters Xevo™ QTof MS mass spectrometer (Waters, Milford, MA, USA), the relative content of the following CER(NS) species in the lipid extract was analyzed: C14-CER[NS], C16-CER[NS], C18-CER[NS], C20-CER[NS], C22-CER[NS], C24-CER[NS], C24:1-CER[NS], and C26-CER[NS], with Avanti Polar Lipids (Alabaster, AL, USA) being set as standard. Chromatographic separation was performed in a positive mode consisting of phase A (water:7 mM HCOONH4 = 100:2) and phase B (MeOH: 5 mM HCOONH4 = 500:1).

### Immunohistochemistry (IHC)

The expression of filaggrin and loricrin in mouse skin samples was evaluated using IHC. Tissue sections (4 μm thick) were first blocked in PBS containing 2% fetal bovine serum and 0.15% Tween-20 for 30 min at room temperature. After incubation with primary antibodies (rabbit polyclonal against filaggrin; Abcam, cat. No. ab24584, 1:1000; rabbit polyclonal against loricrin: Abcam, cat. No. ab198994, 1:200) overnight at 4°C, Tissue sections were incubated with secondary antibodies for 1.5 h at room temperature. The slides were visualized under a microscope (20× and 40×, Olympus Corp., Tokyo, Japan).

### Statistical analysis

Experimental data was presented as the mean ± standard deviation (SD). $p \leq 0.05$ was considered statistically significant through one-way ANOVA followed by Tukey's tests or Kruskal-Wallis tests using SPSS (version 21.0; IBM Corp., Armonk, NY, USA).

## Results and discussion

### Physical properties of ACF-MN patches

AD is a complex multifactorial skin disease, and the demand for novel therapeutic approaches for relieving AD is increasing. Our previous study developed a novel adipose-derived ECM product ACF and demonstrated the ACF-bonded adipokines exhibited an effective capacity on relieving AD symptoms.[17] To optimize the drug delivery pattern of ACF and increase patient compliance, an MN-mediated ACF delivery strategy was proposed and an ACF-loaded MN patch was manufactured and investigated in the present study. ACF-MNs were fabricated with 10% Gel-MA/1% HA (w/v) solution as carrier of ACF. The ACF/Gel-MA/HA suspension was dispensed into PDMS molds and shaped into ACF-MNs by being placed in vacuum, followed by ultraviolet irradiation, and drying. After casting with a backing solution containing 10% PVA (w/v) and 20% gelatin (w/v), the ACF-MN patches were dried and demolded. Optical microscopy and SEM images

showed that the ACF-MNs were uniformly distributed on the patch (Figure 2(a) and (b)), and the height, base diameter, center-to-center spacing, and tip diameter of the ACF-MN were 960.8 ± 17.65, 452.8 ± 7.940, 982.5 ± 9.035, and 17.56 ± 4.199 μm (mean ± SD; n = 10 each), respectively (Figure 2(c)).

It has been reported that drug loading would weakens MN mechanical strength and decreases the penetration capacity.[34] Therefore, to enable ACF-MNs possess sufficient mechanical strength for skin penetration while to loading as much of the drug as possible, suspensions with different mass ratios of ACF to Gel-MA/HA solution (1:1, 2:1, and 3:1) were fabricated into ACF-MN patches and their fracture forces were measured. *Results showed that the* fracture forces of blank MN, as well as ACF-MNs with 1:1 and 2:1 mass ratio, were 0.09306, 0.09466, and 0.09747 N, respectively, which were enough for pierce through the skin. However, the ACF-MN with a 3:1 mass ratio was not able to generate a fracture force, implying that ACF-MN did not have sufficient mechanical strength to penetrate the skin when the mass ratio of ACF to Gel-MA/HA solution was more than 3:1 (Figure 2(d)). Therefore, the ACF-MN patch with an ACF to Gel-MA/HA solution mass ratio of 2:1 was used in subsequent experiments. Since each microneedle patch contains 200 μl of this mix solution, which indicate that each microneedle patch contains about 133.3 μl ACF.

### Ex vivo skin insertion test and in vitro release profile of ACF-MN patches

In the ex vivo skin insertion test, all the needle tips of ACF-MNs with a 2:1 mass ratio were completely pierced through the mouse skin, and the formed microchannels were further confirmed using trypan blue staining (Figure 2(e)) and H&E staining (Figure 2(f)). One of the most significant advantages of dissolving MNs is their ability to directly deliver drugs into the target skin. The insertion efficiency of MNs effectively affect the drug delivery efficiency and the therapeutic response. In ideal situation, all MNs should be inserted efficiently beneath the skin to achieve an optimal drug delivery and least drug wastage. In the present study, ACF-MN patches were applied to mice skin and left for different time periods (5, 10, 30, and 60 min), and the insertion rate of the needles was measured. As shown in Figure 2(g), the insertion rate significantly increased with the residence time of the ACF-MN patches in the first 30 min, whereas there was no obvious increase in the insertion rate when the residence time was extended from 30 min to 60 min. Additionally, we found that even though the ACF-MN patches have been applied for such a long time (60 min), not all MNs could be left beneath the skin. These results indicated that, although the ACF-MNs had sufficient mechanical strength to penetrate
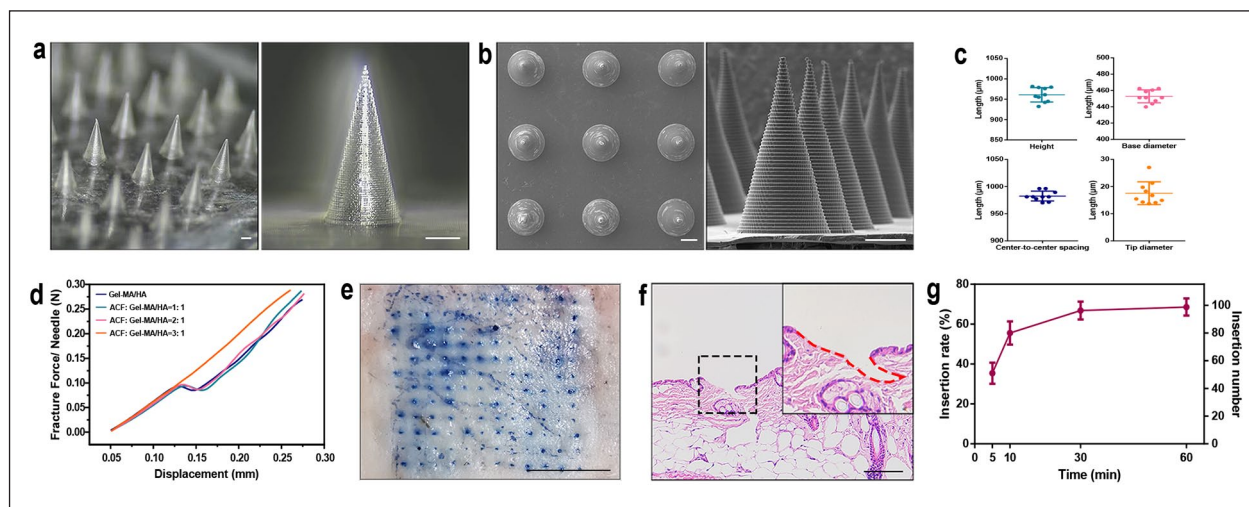
**Figure 2.** Morphology, physical strength, ex vivo skin insertion of ACF-MN patches. (a) Representative optical micrographs of ACF-MN patches. Scale bar: 200 μm. (b) Representative SEM images of ACF-MN patches. Scale bar: 200 μm. (c) Center-to-center spacing, height, base diameter, and tip diameter of ACF-MN ($n=10$, Mean ± SD). (d) Fracture forces of ACF-MNs made of different mass ratios of ACF to Gel-MA/HA solution. (e) Trypan blue staining of the ACF-MN patch-treated mouse skin. (f) H&E staining of ACF-MN patch-treated skin section. (g) Variation tendency of ACF-MN insertion rate with the extension of application time ($n=3$, Mean ± SD).

the skin, not all MNs were successfully left into the skin owing to incomplete separation from the backing layer. Thus, enhancing the insertion efficiency and facilitating the complete insertion of the ACF-MN needle tips into the skin are essential issues to be considered in future studies. Considering the above results of ex vivo skin insertion test, ACF-MN patches were applied for 30 min in the subsequent in vivo experiments.

### In vivo application of ACF-MN patches

To confirm the biosafety and biocompatibility of ACF-MN, ACF-MN patches were applied to the dorsal skin of healthy BALB/c mice. As shown in Figure 3(a), although slight redness and oozing were observed on the dorsal skin of mice immediately after the application of ACF-MN patches, these symptoms gradually subsided, and the dorsal skin of mice rehabilitated to normal state by the seventh day. In addition, there was no obvious adverse effect (e.g. allergies and ulcers) caused by the ACF-MN patches.

Since AD is a chronic recurrent dermatosis, the dissolving MN system of ACF delivery is more rational to be designed as sustained release. To investigate the release pattern of ACF from MN patch in vivo, ACF-MN patches were labeled with Nile red dye and applied to the dorsal skin of BALB/c mice for 30 min, and an in vivo imaging method was used to determine the fluorescence intensity. As shown in Figure 3(b), after in vivo application of the ACF-MN patches, the intensity of the Nile red dye fluorescence gradually decreased from days 0 to 10, and feeble fluorescence was still detected on day 10. Measurement of

fluorescence area showed a decease area in the back of mice from days 0 to 10 (Figure 3(c)). The results indicated that the loading base material Gel-MA/HA could be biodegraded with an appropriate rate that allowed a slow and continuous release of ACF from the MN.

### Therapeutic efficacy of ACF-MN patches on OVA-induced mouse model

To determine the therapeutic effect of ACF-MNs against AD, ACF-MN patches were applied to OVA-induced AD mice, with PBS treatment and freshly made ACF treatment as negative control and positive control, respectively (Figure 4(a)). As shown in Figure 4(b) and (e), compared to the mice without OVA epidermal challenges, repeated sensitization of OVA caused typical dermatitis features (dry desquamation, lichenification, erythema, erosion, and edema) on the mice dorsal skins. Relief of dermatitis features was barely observed in the PBS-treated mice ($13.83 \pm 2.13$, $n=6$), whereas the skin lesions of ACF-MN-treated mice showed significant improvement ($11.00 \pm 1.789$, $n=6$), similar with those of the ACF group ($9.667 \pm 1.751$, $n=6$).

Since AD skin lesions are generally characterized by hyperplasia of epidermis and accumulation of immune cells such as mast cells,[2] H&E and TB staining was performed to evaluate the epidermal thickness and infiltrated mast cells of each group. As shown in Figure 4(c), abnormal thickening of epidermis was observed in the PBS group compared with that of the NC group, whereas ACF-MN treatment significantly alleviated the epidermal
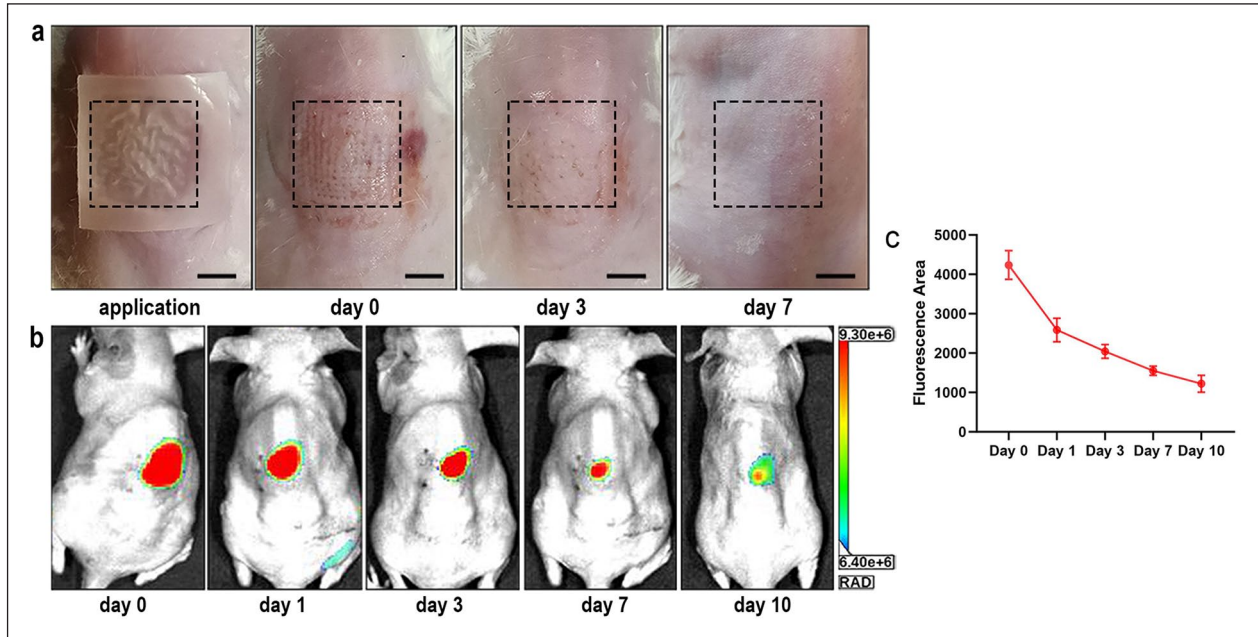
**Figure 3.** In vivo application of ACF-MN patches. (a) Representative images of cutaneous reaction of mice during and after (days 0, 3, and 7) application of ACF-MN patches. Black dotted squares indicate the application sites. Scale bar: 5 mm. (b) Fluorescence image in mouse dorsal skin at different time points (days 0, 1,3, 7, and 10) after application of Nile red dye labeled ACF-MN patches by in vivo imaging. (c) Fluorescence area were measured at the application site on days 0, 1, 3, 7, and 10.

thickening. Statistical analysis showed that the epidermal thickness of ACF group ($27.68 \pm 8.560 \,\mu m$, $n = 10$) and ACF-MN group ($37.66 \pm 20.25 \,\mu m$, $n = 10$) was significantly lower than that of the PBS group ($60.35 \pm 13.96 \,\mu m$, $n = 10$, $p < 0.01$; Figure 3(f)). Moreover, TB staining of skin tissues showed that numerous mast cells infiltrated into the dermis of PBS group ($60.20 \pm 15.98$, $n = 10$). Both of the skin samples from ACF group ($36.20 \pm 8.121$, $n = 10$) and ACF-MN group ($46.70 \pm 12.68$, $n = 10$) exhibited less infiltrated mast cells (Figure 4(d)), which was further confirmed by statistical analysis ($p < 0.05$; Figure 4(g)). These results suggested that ACF-MN patches effectively improved the AD clinical features and pathological changes of OVA-induced AD mouse model similar with ACF.

Taken together, ACF-MN patches practically operated as a device with therapeutic effects on AD skin, as effective as ACF injection, at the microscopic level in in vivo mouse model. Beside the therapeutic use of ACF-MN in AD lesions, it is reasonable to expand the use of ACF-MN in the field of skin aesthetic medicine, since adipokines are beneficial in preventing skin aging.[35,36] In addition, challenges in translating this technology from mice to humans should be concerned. First, randomized controlled clinical trials along with long-term follow-up should be explored to evaluate the safety and efficacy of ACF-MN technique in humans. Second, the patch can be tailored with different length and insertion efficiency, since human skin are diverse in different areas of the body. Third, the condition

of each AD patient is different, thus optimum therapeutic dose and frequency of ACF-MN treatment for each AD patient require investigation.

### Transcriptomic alteration caused by ACF treatment in AD skin lesions

To decipher the mechanisms of the therapeutic effect of ACF on AD, high-throughput RNA-Seq of dorsal skin tissues collected from the NC, PBS, and ACF groups was performed. Based on $|\log2 \, FC| \geq 1$ and $p\text{adj} \leq 0.05$ thresholds, 3908 DEGs were identified among the three groups (Figure 5(a)). In PBS versus NC groups, 1030 upregulated genes and 1201 downregulated genes were identified (Figure 5(b)). In ACF versus PBS group, 520 upregulated genes and 631 downregulated genes were identified (Figure 5(c)).

*ACF down-regulated inflammatory signals in AD skin lesions.* In the initiation of innate immune responses of AD, the pattern recognition receptors, especially Toll like receptors (TLRs) expressed on the surface of keratinocytes and antigen presenting cells are stimulated to initiate the subsequent inflammatory responses.[37] AD is commonly known as a Th2/Th22-mediated inflammatory dermatosis,[38] whereas Th1/Th17-mediated inflammation also exists in some subsets.[39] Especially, IL-17 expression used to be found increased in AD mouse models.[40] In the present study, KEGG analysis showed that the DEGs in PBS
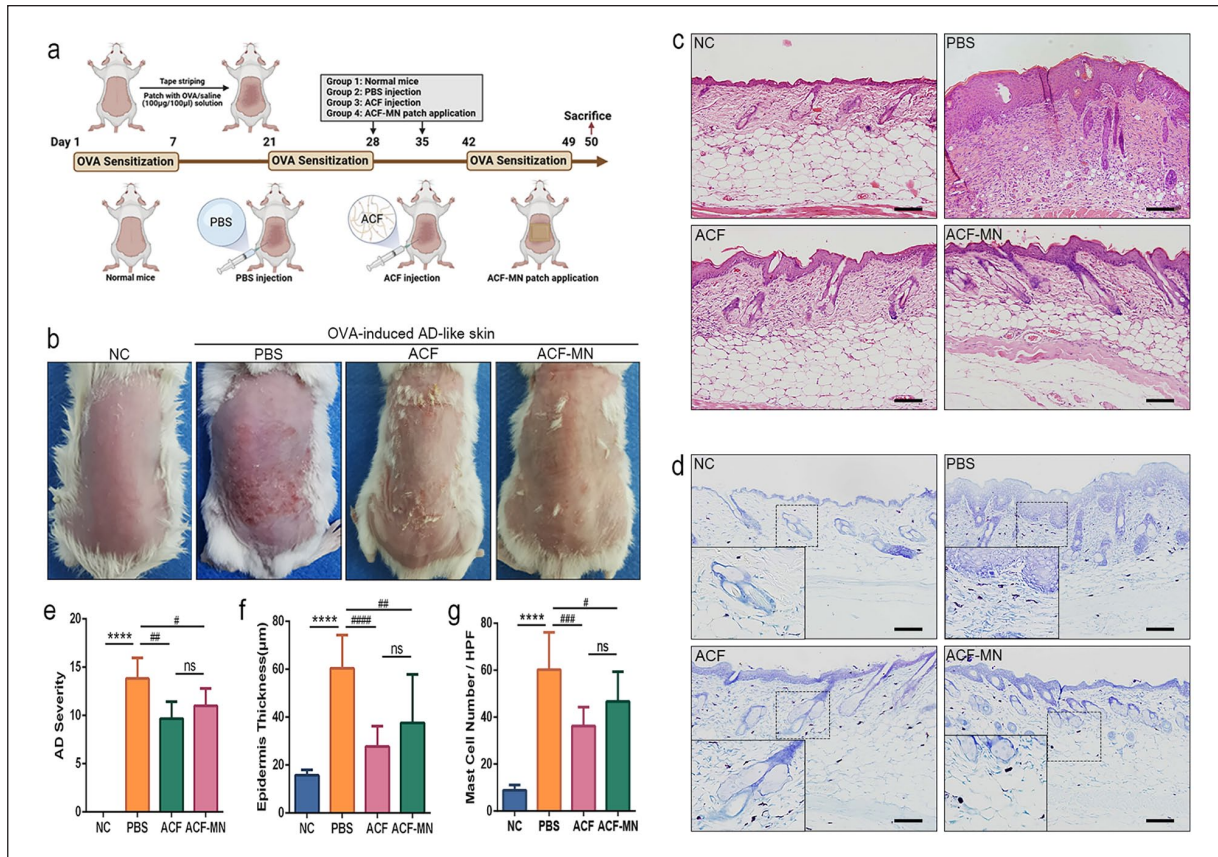
**Figure 4.** Therapeutic effect of ACF-MN patches on OVA-induced AD mice. (a) Schematic of AD mouse model sensitized by OVA solution and application of ACF-MN patches. (b) Representative photographs of mice dorsal skins of the NC, PBS, ACF, and ACF-MN groups on day 50. (c) Representative H&E staining images of mice dorsal skin sections from the four groups. Scale bar: 50 μm. (d) Representative TB staining images of mice dorsal skin sections from the four groups. Scale bar: 50 μm. (e) Statistical comparison of AD severity among groups ($n = 6$, Mean ± SD). (f) Statistical comparison of epidermal thickness among groups ($n = 10$, Mean ± SD). (g) Statistical comparison of infiltrated mast cell number among groups ($n = 10$, Mean ± SD).
****, $p < 0.0001$ compare with NC group. #, $p < 0.05$; ##, $p < 0.01$; ###, $p < 0.001$; ####, $p < 0.0001$ compare with PBS group. One-way ANOVA followed by Turkey's test.

versus NC group were most significantly enriched in inflammation-related pathways "cytokine-cytokine receptor interaction" and "IL-17 signaling pathways" (Figure 5(d), yellow mark). Additionally, GSEA and sample cluster analyses showed that most of the core enrichment genes or/and DEGs involved in the pathways mentioned above were upregulated in the skin samples from PBS group (Figure 5(f) and (g)), indicating an elevated inflammatory level in AD skin lesions. Interestingly, as shown in the KEGG analysis of the DEGs in ACF versus PBS group, "cytokine-cytokine receptor interaction" was also the most significantly enriched pathway (Figure 5(e), yellow mark). In the meanwhile, further sample cluster analyses showed that most of the DEGs involved in this pathway were downregulated from the skin samples of ACF group (Figure 5(h)), suggesting a broad-spectrum inhibiting effect of ACF on AD inflammatory responses. Furthermore, in line with the bioinformatics results, higher expression levels of Th17-type (IL-17), Th2-type (IL-4, IL-13) as well as

Th1-type (TNF-α) cytokines were detected in the skin samples of PBS group compared to those of NC group by qPCR ($p < 0.05$). And the expression levels of these cytokines in ACF group were decreased in varying degrees compared with those of the PBS group ($p < 0.05$; Figure 5(i)), which further confirmed the anti-inflammatory effect of ACF in AD.

The ELISA test was used to evaluate the anti-inflammatory and immunomodulatory effects of ACF extract on RAW264.7 cells. The concentrations of TNF-α and IL-6 were lower in the control group compared with that in the positive control and the microneedle groups. Notably, significant differences were observed between the microneedle group loaded with ACF and the positive control groups ($p < 0.05$; Figure 4(f) and (g)), demonstrating its anti-inflammatory properties.

*ACF modulated microbiota imbalance in AD skin lesions.* Previous studies have suggested that microbiota imbalance is
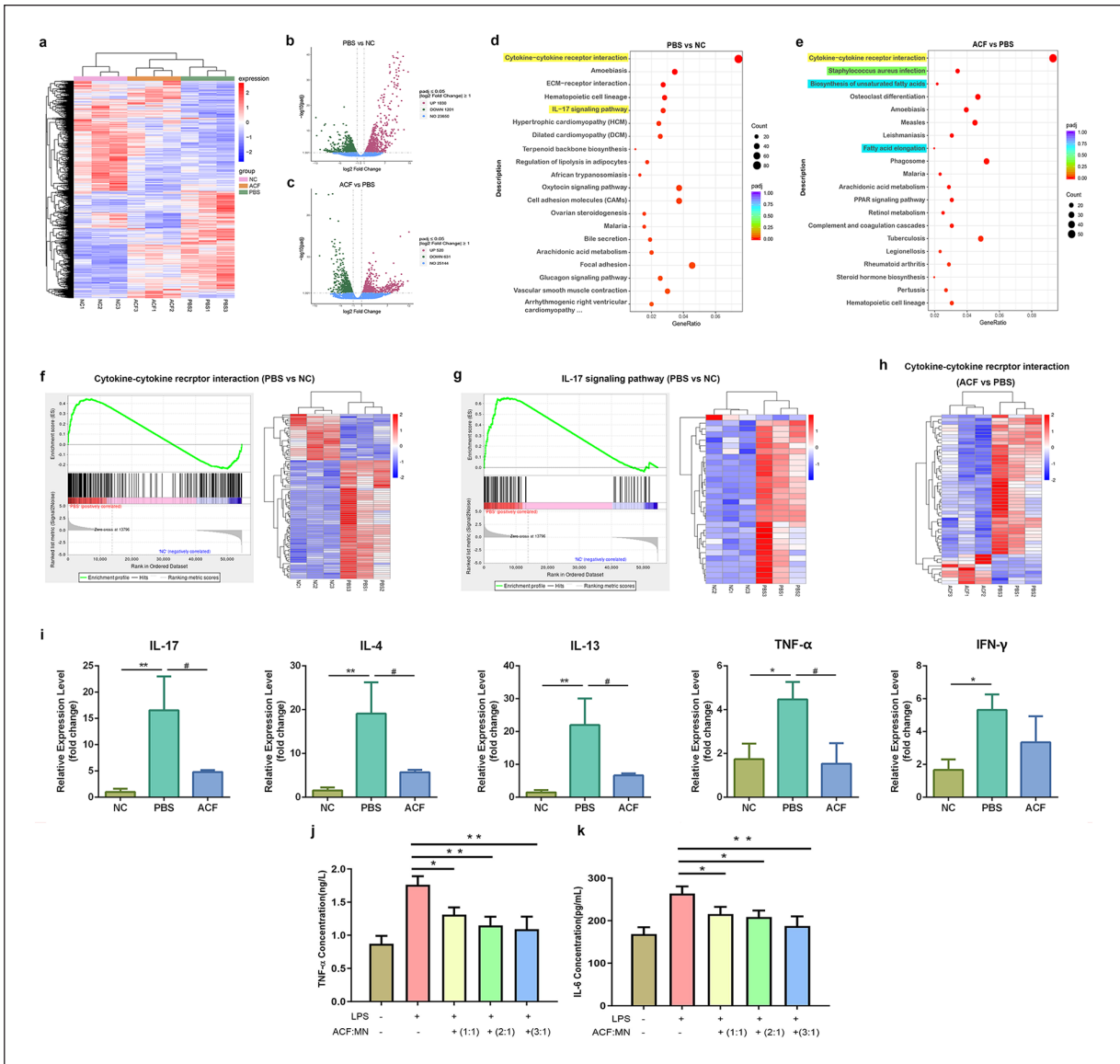
**Figure 5.** RNA-Seq of mice dorsal skin samples and evaluation of the anti-inflammatory ability of ACF on OVA-induced AD mice and RAW264.7 cells. (a) Heat maps of DEGs among NC, PBS, and ACF groups (*n* = 3). (b) Volcano plot of DEGs between the PBS and NC groups. (c) Volcano plot of DEGs between the ACF and PBS groups. (d) KEGG analyses of DEGs in the PBS versus NC group. (e) KEGG analysis of DEGs in the ACF versus PBS group. (f) GESA and sample cluster analyses of "cytokine-cytokine receptor interaction" pathway in PBS versus NC group. (g) GESA and sample cluster analyses of "IL-17 signaling pathways" in PBS versus NC group. (h) Sample cluster analyses of "cytokine-cytokine receptor interaction" pathway in ACF versus PBS group. (i) Relative gene expression levels of IL-17, IL-4, IL-13, TNF-α, and IFN-γ in skin samples of NC, PBS, and ACF groups measured by qPCR (*n* = 6, Mean ± SD). *, $p < 0.05$; **, $p < 0.01$ compare with NC group. #, $p < 0.05$ compare with PBS group. One-way ANOVA followed by Turkey's test. (j–k) TNF-α and IL-6 concentrations in RAW264.7 cells in each group.*, $p < 0.05$; **, $p < 0.01$.

involved in the pathogenesis of AD. In particular, both antimicrobial peptides and skin microbiome diversity are reduced, and the abundance of *Staphylococcus* increases in AD lesions,[41,42] resulting in an increased susceptibility to skin infections.[43–45] In this study, the DEGs of ACF versus PBS group were also found significantly enriched in the "*Staphylococcus aureus* infection" pathway (Figure 5(e), yellow mark). In addition, GSEA results and sample cluster analyses of this pathway showed that all the core

enrichment genes and/or DEGs were downregulated in ACF group (Figure 6(a)), indicating the antibacterial effect of ACF.

Therefore, 16S-targeted amplicon sequencing was performed to further validate the effect of ACF on AD skin microbiome. The results showed that microbiome richness in PBS-treated mice (190.1 ± 38.85, *n* = 3) was significantly lower than that in normal mice (625.5 ± 25.53, *n* = 3, *p* < 0.001), indicating a loss of skin microbiome
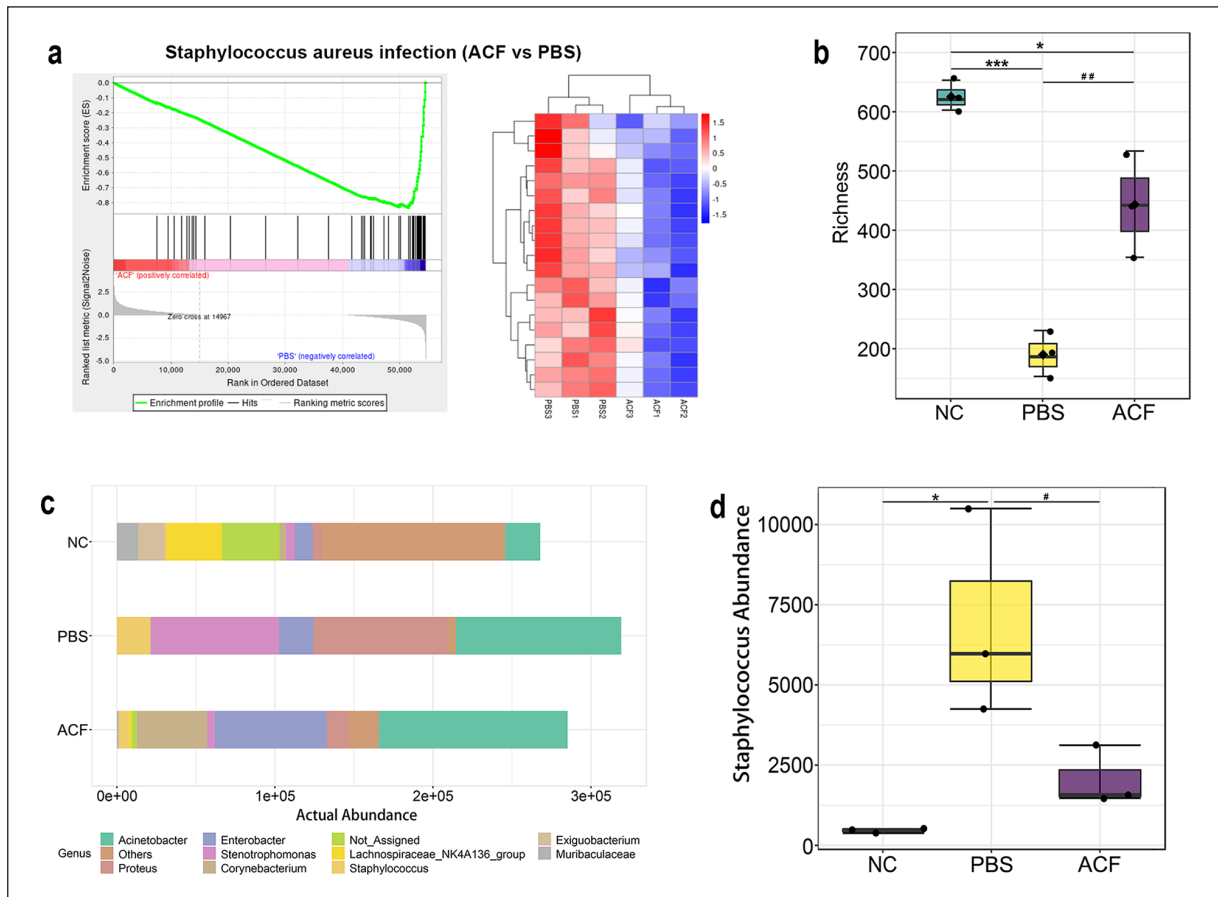
**Figure 6.** The effect of ACF on skin microbiome of OVA-induced AD mice. (a) GESA and sample cluster analyses of "Staphylococcus aureus infection" pathway in ACF versus PBS group. (b) Richness of skin microbiome in NC, PBS, and ACF groups measured by α-diversity analysis ($n = 3$, Mean $\pm$ SD). (c) Taxonomy analysis of taxa actual abundance of the three groups displayed at genus level ($n = 3$). (d) Abundance of Staphylococcus in the three groups ($n = 3$, Mean $\pm$ SD). *, $p < 0.05$; ***, $p < 0.001$ compare with NC group. #, $p < 0.05$; ##, $p < 0.01$ compare with PBS group. One-way ANOVA followed by Turkey's test.

diversity in AD skin lesions. Nevertheless, the richness of skin microbiome increased to some extent in ACF-treated mice ($443.4 \pm 89.69$, $n = 3$, $p < 0.01$), suggesting the restoration of microbiome diversity after ACF treatment (Figure 6(b)). At the genus level, the abundance of *Staphylococcus* in PBS group ($6875 \pm 3174$, $n = 3$) was higher than that in NC group ($457.7 \pm 70.50$, $n = 3$, $p < 0.05$), whereas ACF group ($2055 \pm 924.4$, $n = 3$, $p < 0.05$) showed a decreased level of the abundance of *Staphylococcus* compared to that of the PBS group (Figure 6(c) and (d)). These results indicated that ACF treatment inhibited the expansion of *Staphylococcus* population in AD skin lesions. Recent studies have shown that *Staphylococcus* strains colonizing patients with AD are prone to biofilm production,[46–48] which creates a protective environment that favors the colonization of new microbes and enhances resistance to antimicrobial therapy.[49,50] In the present study, ACF-MN patches could overcome the biofilms barrier by direct physical penetration without intense pain. Simultaneously, ACF-MNs provided a sustained release of therapeutic adipokines and might prevent the recurrence of infection and biofilm formation.

*ACF improved lipid synthesis dysregulation in AD skin lesions.* AD skin lesion is characterized by epidermal barrier defects, which triggers easy access of pathogens, allergens, and external pollutants,[51] and causes an increase in TEWL.[52] Lipid species, especially ceramides, are the major constituents of epidermal layer and crucial in maintaining skin barrier function. Patients with AD usually show a decrease of epidermal lipid content as well as dysregulation of lipid species.[53–55] In the present study, KEGG analysis of ACF versus PBS group showed that lipid biosynthesis-related pathways were significantly enriched, including "biosynthesis of unsaturated fatty acids" and "fatty acid elongation" (Figure 5(e), blue mark). Furthermore, GESA results as well as sample cluster analyses showed that most of the core enrichment genes and/or DEGs were upregulated in ACF group (Figure 7(a)), indicating that ACF treatment might be able to improve the synthesis and elongation of fatty acids in AD skin lesions.

In healthy human epidermal, ceramides are primarily composed of species with very long chain fatty acids (C16–C36, mainly C24). In the process of >C16 fatty acids elongation, condensation reaction is the
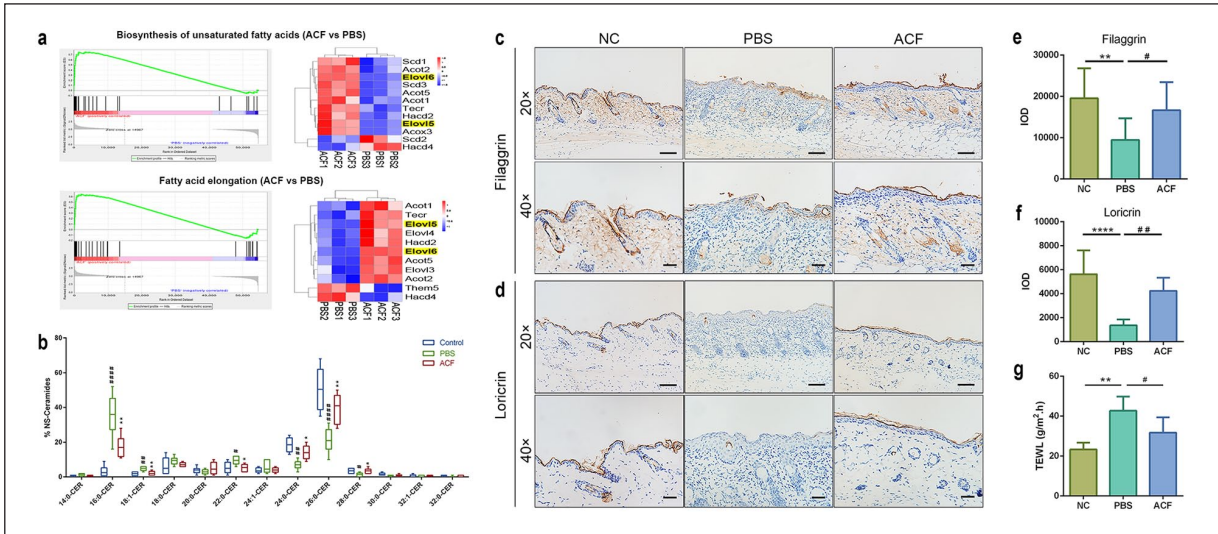
**Figure 7.** Evaluation of the skin barrier repair capability of ACF on OVA-induced AD mice. (a) GESA and sample cluster analyses of "Biosynthesis of unsaturated fatty acids" and "Fatty acid elongation" pathways in ACF versus PBS group. (b) Skin NS-ceramide composition in NC, PBS, and ACF group evaluated by LC-MS. (c) Representative IHC staining images of filaggrin in the three groups. (d) Representative IHC staining images of loricrin in the three groups. Scale bar: 50 μm (upper); 20 μm (lower). (e) Expression level of filaggrin using image J software ($n = 10$, Mean $\pm$ SD). (f) Expression level of loricrin using image J software ($n = 10$, Mean $\pm$ SD). (g) TEWL of mice dorsal skins in the three groups ($n = 6$, Mean $\pm$ SD). **, $p < 0.01$; ****, $p < 0.0001$ compare with NC group. #, $p < 0.05$; ##, $p < 0.01$ compare with PBS group. One-way ANOVA followed by Turkey's test.

rate-limiting step, which is catalyzed by FA elongases with seven isozymes (ELOVL1–7). As shown in the sample cluster analyses of "biosynthesis of unsaturated fatty acids" and "fatty acid elongation" pathways, the genes Elovl5 and Elovl6, which encodes the isozymes ELOVL5 and ELOVL6, were upregulated in ACF group (Figure 7(a), yellow mark). Thereafter, using LC-MS technique, the ceramide species of the three groups were detected. The results showed that compared with NC group, dysregulation of skin ceramide species occurred in PBS group, which reflected as reduction of ceramide species bonded with long chain fatty acids accompanied with increase of ceramide species bonded with short chain fatty acids. Whereas, the skin ceramide composition was normalized in ACF group compared with that of the PBS group (Figure 7(b)).

Next, we evaluated the skin barrier integrity via TEWL as well as IHC staining. It has been established that the impaired skin barrier function is mainly attributed to downregulation of epidermal differentiation-related proteins, such as filaggrin[56] and loricrin.[57] As shown in the IHC results (Figure 7(c)–(f)), the IOD of filaggrin and loricrin in PBS group (filaggrin: $9460 \pm 5252$; loricrin: $1362 \pm 489$) was lower than that in NC group (filaggrin: $19,566 \pm 7248$, $p < 0.01$; loricrin: $5624 \pm 1998$, $p < 0.0001$). In contrast, increased expression level of these two proteins was found in ACF group compared with those in PBS group (filaggrin: $16,658 \pm 6785$, $p < 0.05$; loricrin: $4237 \pm 1104$, $p < 0.01$). In the meanwhile, the TEWL level in ACF group ($31.72 \pm 7.714$, $n = 6$) was

significantly lower than that in PBS group ($42.68 \pm 7.108$, $n = 6$, $p < 0.05$; Figure 7(g)). These results indicated that ACF treatment normalizes lipid species synthesis and facilitates the repair of the skin barrier in AD skin lesions.

## Conclusion

AD is a complex multifactorial skin disease, and the demand for novel therapeutic approaches for relieving AD is increasing. In our previous study, a novel physically extracted adipose-derived ECM namely ACF was illustrated as a candidate for AD treatment benefited by multiple sustained release adipokines. In the present study, in order to comfort the pain generated from conventional intradermal injection, we improve the ACF delivery strategy and developed an ACF-loaded MN patch using Gel-MA/HA. ACF-MN with an ACF to Gel-MA/HA solution mass ratio of 2:1 was confirmed to be fabricated with a uniform shape and sufficient physical strength that could be stably inserted into the skin with minimal side effects. In in vivo experiments, ACF-MN patch was determined sufficient for alleviating skin inflammation in the AD-like skin lesions, similar to ACF injection. Furthermore, using RNA-Seq technique combined with corresponding testing items, we preliminarily clarified a comprehensive therapeutic effect of ACF on AD through modulating immune disorder, microbiota imbalance, and lipid synthesis dysregulation. Thus, we believe that ACF-MN patch developed in this study may serve as a promising delivery strategy that alternating conventional ACF injection for

relieving AD. However, our RNA-Seq analysis only provides a preliminary insights in ACF therapy, a deeper exploration or confirmation of the specific pathways and genes affected by ACF treatment on AD should be considered in further studies. In particular, additional molecular biology techniques should be applied to explore the underlying mechanisms of this adipose-derived therapy on modulating microbiota imbalance and normalizing lipid species synthesis in AD lesions to bolster our conclusions. Furthermore, ACF as well as ACF-MN patch would be a candidate for relieving other inflammatory dermatoses which involve similar pathogenesis, such as psoriasis and eczema, especially in chronic phase. Further studies are needed to optimize the therapeutic dosage of ACF in MN-patches. Additionally, further investigation on ACF-MN patches in large animal models could allow us to understand clinical translation aspects in greater depth.

### Data availability statement

The data that support the findings of this study are available from the corresponding author upon reasonable request.

### Declaration of conflicting interests

The author(s) declared no potential conflicts of interest with respect to the research, authorship, and/or publication of this article.

### Funding

### ORCID iDs

Jingyan Guan [iD] https://orcid.org/0000-0003-0641-7352
Yunfan He [iD] https://orcid.org/0000-0002-5681-4666

### References

1. Thaçi D, Simpson EL, Beck LA, et al. Efficacy and safety of dupilumab in adults with moderate-to-severe atopic dermatitis inadequately controlled by topical treatments: a randomised, placebo-controlled, dose-ranging phase 2b trial. *Lancet* 2016; 387: 40–52.

2. Langan SM, Irvine AD and Weidinger S. Atopic dermatitis. *Lancet (London, England)* 2020; 396: 345–360.

3. Leung DYM. New insights into atopic dermatitis: role of skin barrier and immune dysregulation. *Allergol Int* 2013; 62: 151–161.

4. Brunner PM, Khattri S, Garcet S, et al. A mild topical steroid leads to progressive anti-inflammatory effects in the skin of patients with moderate-to-severe atopic dermatitis. *J Allergy Clin Immunol* 2016; 138: 169–178.

5. Bieber T. Atopic dermatitis: an expanding therapeutic pipeline for a complex disease. *Nat Rev Drug Discov* 2022; 21: 21–40.

6. Bieber T. Disease modification in inflammatory skin disorders: opportunities and challenges. *Nat Rev Drug Discov* 2023; 22: 662–680.

7. Saeki H, Nakahara T, Tanaka A, et al. Clinical practice guidelines for the management of atopic dermatitis 2016. *J Dermatol* 2016; 43: 1117–1145.

8. Weidinger S, Beck LA, Bieber T, et al. Atopic dermatitis. *Nat Rev Dis Primers* 2018; 4: 1.

9. Fölster-Holst R, Torrelo A, Das K, et al. Biological medication in atopic dermatitis. *Expert Opin Biol Ther* 2022; 22: 643–649.

10. de Bruin-Weller M, Thaci D, Smith CH, et al. Dupilumab with concomitant topical corticosteroid treatment in adults with atopic dermatitis with an inadequate response or intolerance to ciclosporin A or when this treatment is medically inadvisable: a placebo-controlled, randomized phase III clinical trial (LIBERTY AD CAFE). *Brit J Dermatol* 2018; 178: 1083–1101.

11. Fasshauer M and Blüher M. Adipokines in health and disease. *Trends Pharmacol Sci* 2015; 36: 461–470.

12. Taylor EB. The complex role of adipokines in obesity, inflammation, and autoimmunity. *Clin Sci* 2021; 135: 731–752.

13. Halberg N, Wernstedt-Asterholm I and Scherer PE. The adipocyte as an endocrine cell. *Endocrinol Metab Clin North Am* 2008; 37: 753–768.

14. Kim EJ, Kim YK, Kim MK, et al. UV-induced inhibition of adipokine production in subcutaneous fat aggravates dermal matrix degradation in human skin. *Sci Rep* 2016; 6: 25616.

15. Zhang Y, Zhang X, Jin X, et al. Adipose collagen fragment: a novel adipose-derived extracellular matrix concentrate for skin filling. *Aesthet Surg J* 2021; 42(5): NP337–NP350.

16. Jin X, Zhang Y, Zhang X, et al. An adipose-derived injectable sustained-release collagen scaffold of adipokines prepared through a fast mechanical processing technique for preventing skin photoaging in mice. *Front Cell Dev Biol* 2021; 9: 722427.

17. Guan J, Feng J, Xu M, et al. Adipokines-enriched adipose extract restores skin barrier and ameliorates inflammatory dysregulation in an atopic dermatitis mouse model. *Plast Reconstr Surg* 2024; 154(4): 701e–712e.

18. Jung HM, Eun SH, Lee JH, et al. Less painful and effective intralesional injection method for lichen simplex chronicus. *J Am Acad Dermatol* 2018; 79: e105–e106.

19. Ning X, Wiraja C, Chew WTS, et al. Transdermal delivery of Chinese herbal medicine extract using dissolvable microneedles for hypertrophic scar treatment. *Acta Pharm Sin B* 2021; 11: 2937–2944.

20. Cui M, Wiraja C, Chew SWT, et al. Nanodelivery systems for topical management of skin disorders. *Mol Pharm* 2021; 18: 491–505.

21. Yang D, Chen M, Sun Y, et al. Microneedle-mediated transdermal drug delivery for treating diverse skin diseases. *Acta Biomater* 2021; 121: 119–133.

22. Qu F, Geng R, Liu Y, et al. Advanced nanocarrier- and microneedle-based transdermal drug delivery strategies for skin diseases treatment. *Theranostics* 2022; 12: 3372–3406.

23. Ben DN, Richtman Y, Gross A, et al. Design and evaluation of dissolvable microneedles for treating atopic dermatitis. *Pharmaceutics* 2023; 15: 1109.

24. Zhang J, Li H, Albakr L, et al. Microneedle-enabled therapeutics delivery and biosensing in clinical trials. *J Control Release* 2023; 360: 687–704.

25. Bandyopadhyay M, Morelli AE, Balmert SC, et al. Skin codelivery of contact sensitizers and neurokinin-1 receptor antagonists integrated in microneedle arrays suppresses allergic contact dermatitis. *J Allergy Clin Immunol* 2022; 150(1): 114–130.

26. Jang M, Kang BM, Yang H, et al. High-dose steroid dissolving microneedle for relieving atopic dermatitis. *Adv Healthc Mater* 2021; 10: 2001691.

27. Ohn J, Jang M, Kang BM, et al. Dissolving candlelit microneedle for chronic inflammatory skin diseases. *Adv Sci* 2021; 8: 2004873.

28. Nazary AF, Salimi L, Saghati S, et al. Application of microneedle patches for drug delivery; doorstep to novel therapies. *J Tissue Eng* 2022; 13: 1768575694.

29. Donnelly RF, Raj ST and Woolfson AD. Microneedle-based drug delivery systems: microfabrication, drug delivery, and safety. *Drug Deliv* 2010; 17: 187–207.

30. Zhu J, Zhou X, Kim HJ, et al. Gelatin methacryloyl microneedle patches for minimally invasive extraction of skin interstitial fluid. *Small* 2020; 16: e1905910.

31. Song JH, An EJ, Sung CY, et al. A comparative study on a biodegradable hyaluronic acid microneedle patch with a needleless patch for dry skin in atopic dermatitis: a single-blinded, split-body, randomized controlled trial. *Arch Dermatol Res* 2023; 315: 569–581.

32. Spergel JM, Mizoguchi E, Brewer JP, et al. Epicutaneous sensitization with protein antigen induces localized allergic dermatitis and hyperresponsiveness to methacholine after single exposure to aerosolized antigen in mice. *J Clin Invest*. 1998; 101: 1614–1622.

33. Nemoto S, Nakamura M, Osawa Y, et al. Sphingosine kinase isoforms regulate oxaliplatin sensitivity of human colon cancer cells through ceramide accumulation and akt activation. *J Biol Chem* 2009; 284: 10422–10432.

34. Tuan-Mahmood T, McCrudden MTC, Torrisi BM, et al. Microneedles for intradermal and transdermal drug delivery. *Eur J Pharm Sci* 2013; 50: 623–637.

35. Yang S, Sun Y and Yan C. Recent advances in the use of extracellular vesicles from adipose-derived stem cells for regenerative medical therapeutics. *J Nanobiotechnol* 2024; 22: 316.

36. Deng M, Xu Y, Yu Z, et al. Protective effect of fat extract on UVB-induced photoaging in vitro and in vivo. *Oxid Med Cell Longev* 2019; 2019: 6146942.

37. Kuo I, Yoshida T, De Benedetto A, et al. The cutaneous innate immune response in patients with atopic dermatitis. *J Allergy Clin Immunol* 2013; 131: 266–278.

38. Krueger JG, Fretzin S, Suarez-Farinas M, et al. IL-17A is essential for cell activation and inflammatory gene circuits in subjects with psoriasis. *J Allergy Clin Immunol* 2012; 130: 145–154.

39. Dhingra N and Guttman-Yassky E. A possible role for IL-17A in establishing Th2 inflammation in murine models of atopic dermatitis. *J Invest Dermatol* 2014; 134: 2071–2074.

40. Oyoshi MK, Wang JYT and Geha RS. Immunization with modified vaccinia virus Ankara prevents eczema vaccinatum in a murine model of atopic dermatitis. *J Allergy Clin Immunol* 2011; 128: 890–892.

41. Tay A, Li C, Nandi T, et al. Atopic dermatitis microbiomes stratify into ecologic dermotypes enabling microbial virulence and disease severity. *J Allergy Clin Immunol* 2021; 147: 1329–1340.

42. Tian X, Huang Q, Liang J, et al. A review of the mechanisms of keratinocytes damage caused by Staphylococcus aureus infection in patients with atopic dermatitis. *J Leukoc Biol* 2021; 110: 1163–1169.

43. Harris-Tryon TA and Grice EA. Microbiota and maintenance of skin barrier function. *Science* 2022; 376: 940–945.

44. Byrd AL, Belkaid Y and Segre JA. The human skin microbiome. *Nat Rev Microbiol* 2018; 16: 143–155.

45. Schommer NN and Gallo RL. Structure and function of the human skin microbiome. *Trends Microbiol* 2013; 21: 660–668.

46. Sonesson A, Przybyszewska K, Eriksson S, et al. Identification of bacterial biofilm and the Staphylococcus aureus derived protease, staphopain, on the skin surface of patients with atopic dermatitis. *Sci Rep* 2017; 7: 8689.

47. Allen HB, Vaze ND, Choi C, et al. The presence and impact of biofilm-producing staphylococci in atopic dermatitis. *Jama Dermatol* 2014; 150: 260–265.

48. Blicharz L, Michalak M, Szymanek-Majchrzak K, et al. The propensity to form biofilm in vitro by staphylococcus aureus strains isolated from the anterior nares of patients with atopic dermatitis: clinical associations. *Dermatology* 2021; 237: 528–534.

49. Tomasek JJ, Gabbiani G, Hinz B, et al. Myofibroblasts and mechano-regulation of connective tissue remodelling. *Nat Rev Mol Cell Bio* 2002; 3: 349–363.

50. Edwards R and Harding KG. Bacteria and wound healing. *Curr Opin Infect Dis* 2004; 17: 91–96.

51. Proksch E, Brandner JM and Jensen JM. The skin: an indispensable barrier. *Exp Dermatol* 2008; 17: 1063–1072.

52. Hon KL, Leung AK and Barankin B. Barrier repair therapy in atopic dermatitis: an overview. *Am J Clin Dermatol* 2013; 14: 389–399.

53. Imokawa G. A possible mechanism underlying the ceramide deficiency in atopic dermatitis: expression of a deacylase enzyme that cleaves the N-acyl linkage of sphingomyelin and glucosylceramide. *J Dermatol Sci* 2009; 55: 1–9.

54. Imokawa G, Abe A, Jin K, et al. Decreased level of ceramides in stratum corneum of atopic dermatitis: an etiologic factor in atopic dry skin? *J Invest Dermatol* 1991; 96: 523–526.

55. Elias PM. Lipid abnormalities and lipid-based repair strategies in atopic dermatitis. *Biochim Biophys Acta* 2014; 1841: 323–330.

56. Howell MD, Kim BE, Gao P, et al. Cytokine modulation of atopic dermatitis filaggrin skin expression. *J Allergy Clin Immunol* 2009; 124: R7–R12.

57. Kim BE, Leung DYM, Boguniewicz M, et al. Loricrin and involucrin expression is down-regulated by Th2 cytokines through STAT-6. *Clin Immunol* 2008; 126: 332–337.